Axonopathy is a compounding factor in the pathogenesis of Krabbe disease.

Ludovico Cantuti Castelvetri • Maria Irene Givogri • Hongling Zhu • Benjamin Smith • Aurora Lopez-Rosas • Xi Qiu • Richard van Breemen • and Ernesto Bongarzone

L. Cantuti Castelvetri and M.I. Givogri contributed equally to this work.

L. Cantuti Castelvetri • M.I. Givogri • H. Zhu • B. Smith • A. Lopez-Rosas • E. Bongarzone (✉)

Department of Anatomy and Cell Biology, College of Medicine, University of Illinois, Chicago. 808 South Wood Street. MC512. Chicago, IL. 60612.

Email: ebongarz@uic.edu

X. Qiu • R. van Breemen

Department of Medicinal Chemistry and Pharmacognosy, College of Pharmacy, University of Illinois, Chicago, 833 South Wood Street. MC 874

Running Title: Dying back axonopathy in Krabbe disease.

ABSTRACT

Loss-of-function of the lysosomal enzyme galactosyl-ceramidase (GALC) causes the accumulation of the lipid raft-associated sphingolipid psychosine, the disruption of postnatal myelination, neurodegeneration and early death in most cases of infantile Krabbe disease. This work presents a first study towards understanding the progression of axonal defects in this disease using the Twitcher mutant mouse. Axonal swellings were detected in axons within the mutant spinal cord as early as one week after birth. As the disease progressed, more axonopathic profiles were found in other regions of the nervous system, including peripheral nerves and various brain areas. Isolated mutant neurons recapitulated axonal and neuronal defects in the absence of mutant myelinating glia, suggesting an autonomous neuronal defect. Psychosine was sufficient to induce axonal defects and cell death in cultures of acutely isolated neurons. Interestigly, axonopathy in young Twitcher mice occured in the absence of demyelination and of neuronal apoptosis. Neuronal damage occurred at later stages, when mutant mice were moribund and demyelinated. Altogether, these findings suggest a progressive dying-back neuronal dysfunction in Twitcher mutants.

INTRODUCTION

Inherited pediatric leukodystrophies are monogenetic diseases affecting the metabolism of myelin components [5, 11]. Reasonably, most studies focused on the mechanisms of demyelination. However, there is a significant void in understanting the contribution of neuronal and axonal stress to neuropathology in these diseases. Krabbe disease is a demyelinating lethal leukodystrophy caused by the loss of function of galactosyl-ceramidase (GALC), a lysosomal enzyme participating in galactosyl-sphingolipid degradation, [1, 24, 40, 48]. Psychosine -one of GALC substrates and a lipid raft-associated galactosylsphingolipid [50, 49]- accumulates to toxic levels in these patients, triggering a pathogenic defect in myelinating glial cells and causing progressive demyelination, [26, 42, 53].

Although demyelination is clearly the main hallmark in Krabbe disease, sporadic reports described axonal and neuronal degeneration in autopsy material [2, 17, 30, 37, 39]. Neuronal dysfunction was also described in the Twitcher mutant, the only available natural mouse model of Krabbe disease, [15, 19, 20, 35]. Unfortunately, the mechanism of neurodegeneration remained uncharacterized.

Understanding the functional impact of neurodegeneration is highly relevant to design efficient therapies for Krabbe disease. Currently, some patients benefit from enzyme reconstitution by cross-correction of GALC in myelinating glia, after transplantation of bone marrow or hematopoietic stem cells from healthy donors. In the Twitcher, this approach takes about 30-50 days to achieve significant enzyme levels in the brain [23]. This leaves the nervous system with minimal correction during a critical time of postnatal development.

Although the general consensus is that axonal degeneration is secondary to demyelination, whether or not GALC-deficient neurons are defective and when this defect

starts is unknown. If mutant neurons are also affected by the metabolic blockage in Krabbe disease, this defect may limit the clinical value of current therapeutic interventions, which are primarily aiming to correct myelinating glia. This first study characterizes axonal and neuronal damage in the Twitcher mouse, focusing on the mutant spinal cord motor neurons and nerve fibers in the sciatic nerve.

MATERIALS AND METHODS

Animals. Breeder Twitcher heterozygous mice (C57BL/6J, twi/+) and Thy1.1:YFP H+/+ mice (Jackson Laboratory, Bar Harbor, ME) were maintained under standard housing conditions. In vivo experiments were approved by the Animal Care and Use Committee of our institution. Twitcher and Thy1.1:YFP mice were crossed to produce double heterozygous TWI+/- Thy1.1:YFP+/-. Twitcher mice expressing YFP (TWI-YFPax) were identified by PCR as described [16, 18].

Cell cultures. Primary cell cultures of glial cells and neurons have been described in detail elsewhere [3, 6]. NSC34 cells were grown in DMEM supplemented with 5% FBS, L-glutamine (Gibco) and penicillin/streptomycin (Gibco). NSC34 cells were serum deprived for 12 hours before the addition of lipids. Psychosine, D-Sphingosine and C6-Ceramide were purchased from Sigma and resuspended in 0.001% ethanol.

Tissue Collection, histology, and immunohistochemistry. Mice were anesthetized and perfused with saline. Tissues for psychosine determination, and immunoblot were frozen in liquid nitrogen. Tissues for immunohistochemistry and regular histology were postfixed in 4% paraformaldehyde/phosphate buffer saline (PBS) for 18 hr, embedded in sucrose, and frozen in OCT. Appropriate blocks of tissue were separated and processed for electron microscope imaging (see below). Cryosections (20 μm) were mounted onto superfrost slides. For immunofluorescence staining, sections were dried for 15 minutes at 37°C, and washed in PBS. The sections were blocked/permeabilized in 5% bovine serum albumin, 0.5% Triton X-100/PBS for one hour at room temperature and incubated with NeuN (Abcam; 1:100) or CGT (Abcam; 1:100) antibodies diluted in 2% BSA, 0.5% Triton X-100/PBS buffer overnight at 4°C, with mild agitation. Slides were rinsed in PBS and incubated with fluorescent secondary antibodies (Alexa 488) for 1 hour at room temperature, washed in PBS and counterstained with propidium iodide. Mouting was performed with Vectashield (Vector, Burlingame, CA).

Confocal microscopy was performed using a confocal laser Meta Leica scanning microscope. Terminal deoxynucleotidyl transferase dUTP nick end labeling (TUNEL) assay was performed according to the manufacturer instructions (Roche). Briefly, after drying at 37°C and washing in PBS, sections were then permeabilized in 0.1% Triton X-100, 0.1% Na Citrate in PBS for 2 minutes on ice. After rinses in PBS, slides were incubated with terminal transferase and labeled for 60 minutes at 37°C. After rinses in PBS, slides were mounted with permount or the NeuN staining was performed.

Immunofluorescence. Cells were grown on poly-lysine treated coverslips. Cells were washed in PBS, fixed in 4% paraformaldehyde/PBS, permeabilized in 0.1% triton-X and blocked with 4% BSA/PBS. Coverslips were incubated with anti-active caspase 3 diluted in blocking solution at 4°C overnight. After rinses in PBS, coverslips were incubated with Alexa-488 secondary antibody in 4% BSA/PBS, washed and mounted.

Stereology. For unbiased stereological studies, 30-μm-thick spinal cord cross-sections were selected (one every 10 sections) and stained accordingly. Quantification of positive cell markers was performed with design-based stereology system (StereoInvestigator version 8, MBF Bioscience, Williston, VT, USA). Briefly, the spinal cord ventral horns were traced under 5X objective and TUNEL+ motorneurons were counted under 63X objective (Zeiss AX10 microscope, Carl Zeiss Ltd., Hertfordshire, England). The sampling parameters were set up according to the software guide to achieve the coefficient of error ranged between 0.09 and 0.12 using the Gundersen test, normally a counting frame size 100X100 μm, optical dissector height 20 μm, and an average of 10 sampling sites per section were chosen.

Gene expression analysis. RNA from cultured cortical neurons was purified with Trizol (Invitrogen), according to the manufacturerfs instructions. The quality of the RNA was determined by measuring the absorbance at 260 and 280 nm. Retrotranscription was performed with the Superscript III (Invitrogen) according to the manufacturer instructions.

Real Time PCR analysis was performed with primers specific for GALC, CGT and the 60S acidic ribosomal protein P0 (RPLP0), that was used as the internal control. The primers were tested on a standard curve and the efficiency and the correlation coefficient were higher than 90% and 0.990, respectively. PCR analysis was calculated with the Delta-delta Ct method. The following primers were used:

GALC Forward: CTGGATACTCTATGGCTCCTTGAC; GALC Reverse: AGTGGTGA GCG TAAATATCTCGTC; CGT Forward: CAATAATCCCAGTTATCGGCAGAG

CGT Reverse: TCCAATAGGTAGTCCGATTGACAG; RPLP0 Forward: CACGAAGCTA ACGACTATCGC RPLP0 Reverse: CTCTAGGGACTCGTTCGTGC

Western blotting. Tissues were homogenized in lysis buffer (1 mM PMSF, 2 mM Sodium Orthovanadate, 1 mM NaF, 20 mM Tris HCl pH 7.4, 1% Triton X100, 150 mM NaCl, 5 mM MgCl$_2$, 300 nM Okadaic acid). Samples were then briefly sonicated on ice and spinned down at 5000 rpm for 5 min to remove debri. Protein concentration in the supernatant was quantified by Bradford assay (Biorad) and equal amount of proteins were loaded on a 4-12% Bis-Tris gel (Invitrogen). SDS-PAGA electrophoresis lasted for 4 hours at 80 mV. Proteins were electrotransferred for 2 hours at 120 v on a PVDF membrane (Biorad). Blots were blocked in 5% milk, 1% BSA, 0.05% Tween 20 in Tris Glycine buffer (blocking solution) and incubated with primary antibodies at 4°C overnight. Secondary peroxidase-conjugated antibodies were added for 1 hour at room temperature. The primary antibodies were: anti actin (Sigma), anti CGT (Abnova), anti GALC (Santa Cruz), anti MBP (Chemicon), and anti P0 (Chemicon) antibodies. Immunoreactions were developed using the Enhanced Luminescence kit (Thermo Scientific). Bands were quantified using NIH free imaging software Image J and normalized to housekeeping proteins.

Psychosine determination. Psychosine was extracted and quantified as previously described [19].

Nissl staining. Sections (30 µm-thick) were treated with 100% ethanol and xylene and then re-hydrated. Slides were immersed in 0.1% cresyl violet (prepared in distilled water and 3% acetic acid) for 5 minutes, before rinses in 1% acetic acid-70% ethanol and 1% acetic acid-100% ethanol and mounting with permount. Deeply stained motoneurons in the ventral horn were counted by stereology as viable Nissl+ cells.

MTT survival assay. MTT assay (Chemicon) was performed as indicated by the supplier, on cultured cells (5000 cells/well) plated in 96 well plates. Stimuli were administered for 24 hours before MTT assay.

Statistical analysis. Where appropriate, results are the average from at least 3 independent experiments and are expressed as the mean ± SE. Data were analyzed by the Student's t test and p values <0.05 were considered statistically significant (*).

RESULTS

Axonal dystrophy in the Twitcher mouse. We crossed the Twitcher line with the reporter line Thy1.1-YFP, which expresses YFP in subsets of motorneurons, allowing the fluorescent labeling of their projecting axons. The new reporter Twitcher mouse line, named Twi-YFPax, permitted an easy, fast and detailed fluorescent characterization of axonal morphology in various neuronal populations from cortex (motor neurons in layers 2-6), cerebellum (some Purkinje neurons), hippocampus, dorsal root ganglia and spinal cord (particularly lower spinal cord motor neurons). The work presented in this report focused on axons within the spinal cord and sciatic nerve fibers.

Confocal analysis showed a decrease in the density of YFP+ axons in the lumbar spinal cord of P30 Twi-YFPax mice. This was particularly evident in ventral white matter (Fig 1a and 1b). In coronal sections, some mutant axons appeared with swellings (insets in Fig. 1a), suggesting local accumulations of YFP. This observation was confirmed by confocal analysis of longitudinal sections of the spinal cord (white arrows in Fig. 1e). Some axons showed breaks or transections (blue arrows in Fig. 1e) suggesting severe structural disruption. Orthogonal confocal analysis demonstrated that these pathologic profiles were abnormal structures contained within axons (Fig. 2a to 2c). Wild type samples were completely devoid of these profiles (Fig. 2d).

Axonopathy starts before the onset of demyelination. Myelination of the central nervous system appears normal in the early postnatal life of the Twitcher mouse. Published studies [33, 41] and our own examination (suppl. Fig. 1a) show that the onset of demyelination occurs within the third and fourth week of postnatal life of Twitcher mice. Examination of Twi-YPFax mutants showed axonal swellings and varicosities already within the ventral white matter as early as P7 (arrows in Fig. 3a-3b), but not in the age-matched controls (not-shown). Axonal

profiles increased in frequency in the spinal cord of older mutants (Fig. 3c-3e) but not in control tissue (Fig. 3f). The appearance of axonal profiles (swellings or varicosities) at such early postnatal ages and in the absence of demyelination suggests unexpected premature neuronal vulnerability in this disease.

Peripheral nerves are affected of axonopathy. The observation of a progressive axonal dystrophy in the spinal cord prompted us to investigate axonal damage in the sciatic nerve, as this nerve carries some of the longest axons. Similarly to what we found in the spinal cord, swellings and varicosities were detected in sciatic nerves. While these were evident at P15 (arrows in Fig. 4b), we could not detect gross morphological changes in axons from P7 mutant nerves (Fig. 4a). Axonal abnormalities became more evident with the onset of demyelination. At P30, axons in the mutant sciatic nerve appeared with multiple swellings and were frequently transected (arrows in Fig. 4c).

Neuronal apoptosis is a late event in the Twitcher mouse. Axonopathy generally precedes apoptotic death. To address whether Twitcher neurons undergo cell death, coronal sections of the lumbar spinal cord from the Twitcher parental line and from wild type littermates were subjected to the TUNEL assay. The TUNEL assay identifies cleavages in DNA, and has served as a traditional detection method for apoptosis [22, 52]. As expected, TUNEL+ glial nuclei were detected in the white matter of symptomatic mutant mice. The frequency of these apoptotic glia in presymptomaic (P7-P15) Twitcher mice was minimal and not significantly different from wild type littermates (Supp. Fig. 1b). However, TUNEL+ glia sharply increased as Twitcher mice developed the disease, reaching stereological significance when mutants passed the onset of the disease (P30) (Supp. Fig. 1b). Figure 5D-5F shows TUNEL+ glial nuclei within the ventral white matter in lumbar spinal cord samples from P30 Twitcher. These

results are in line with previous studies showing apoptotic death of oligodendrocytes in the Twitcher animals, [26, 43].

Notably, numerous large TUNEL+ motorneurons were also detected in the gray matter of Twitcher mice but only when mutants were symptomatic (P30) (Fig. 5b). However, we did not detect any TUNEL+ motorneuron at earlier developmental times (P7 and P15) (Fig. 5a) nor in tissues from wild type littermates at all ages (Fig. 5i-5k). Co-staining for the neuronal nuclear marker (NeuN) confirmed the neuronal nature of these dying cells (Fig. 5c-5e). Stereological counting of TUNEL+ motorneurons confirmed these results (Fig. 5m). Stereological counting of Neu+ showed absence of significant differences between mutant and control littermates at any age (Fig. 5l), suggesting limited or none loss of neuronal structure. Interestingly, apoptotic neurons were mostly localized in the ventral horn of mutant cords and showed cytoplasmic rather than nuclear localization of the TUNEL staining (Fig. 5c). Although the reason for cytoplasmic localization of the TUNEL staining has not been explained, this pattern has been reported for neurons undergoing chromatolysis [29]. To examine this possibility, spinal cords from P7 and P15 Twitcher and wild type littermates were Nissl stainied (Supp. Fig 2a). The Nissl staining labels large stacks of rough endoplasmic reticulum and ribonuclear complexes (also called Nissl bodies), and its disappearance is a known endpoint for neuronal demise, [12]. Stereological counting of Nissl+ motorneurons showed a significant loss (~20%) of healthy (Nissl+) motorneurons as early as P7 (Supp. Fig. 2b) in the mutant cord. This loss increased to about 45% in P15 mutant mice (Supp. Fig. 2b).

Psychosine is present in Twitcher neurons. The early and progressive defect detected in mutant spinal cord motorneurons may be caused by the accumulation of psychosine in these cells. To address this possibility, we first determined expression levels of CGT, the enzyme responsible for the synthesis of psychosine [8], in neurons. Immunohistochemical analysis

revealed detectable levels of CGT expression in motorneurons (arrows Fig. 6a) and as expected, in oligodendroglial cells (not-shown). Immunoblotting and real time PCR analyses also showed CGT expression in protein extracts from NSC34 cells (Fig. 6c) and mRNA isolated from cortical neurons, (Fig. 6d). Neuronal expression of GALC was also confirmed by real time PCR, (Fig. 6d). Altogether, these results show that neurons contain the metabolic components for the potential production of psychosine. Next, we measured levels of neuronal psychosine in granule neurons –which are largely unmyelinated- isolated from Twitcher and wild type brains. High performance liquid chromatography tandem mass spectrometry (LC-MS-MS) showed three fold-increase of psychosine in mutant neurons respect levels in control neurons (Fig. 6e, 6f). Although, psychosine levels were significantly lower in Twitcher neurons than in isolated Twitcher oligodendrocytes (Fig. 6f), they seemed sufficient to induce morphological changes in mutant neurons. Mutant granule neurons were cultured in the absence of myelinating glia for up to 8 days. While control neurons extended delicate and long neurites, and remained healthy for the entire experiment (Fig. 7d), Twitcher neurons showed early signs of distress, including shortening and swelling of neurites by the fifth day of culture and abundant cell death by the end of the first week of incubation (Fig. 7a-c). Because glucosyl-sphingosine (glucopsychosine) and galactosyl-sphingosine (psychosine) show the same ion/mass value in LC-MS-MS, quality controls were performed to control for this possibility. This analysis clearly demonstrated that our methodology distinguishes both sphingolipids and that psychosine but not glucopsychosine was accumulated in the Twitcher nervous system (Supp. Fig. 3).

Psychosine is a pathogenic molecule sufficient to cause neuronal death in the absence of myelinating glia. To test whether psychosine is pathogenic for neurons various experiments were designed. Motorneuron NSC34 cells and cortical neurons isolated from wild

type mice were exposed to exogenous psychosine to determine the effects of this lipid on neurite stability, apoptotic cell death and cell survival. Experiments were conducted for up to 2 hours (NSC34 cells) or 24 hours (cortical neurons) of incubation. First, NSC34 cells were incubated for one hour with 10 μM psychosine or vehicle (0.001% ethanol) before LC-MS-MS analysis of psychosine incorporation in NSC34 cells (Fig. 7e and 7f). Second, NSC34 cells were incubated with 10 μM psychosine for 2 hours and cell morphology studied by real time videomicroscopy. Psychosine was clearly pathogenic, inducing the retraction of neurites in about 80% of NSC34 cells after 2 hours of incubation (Fig. 7g and Supp. Video). Vehicle treatment did not have any effect on neurite stability (Fig. 7g and Supp. Video). Swellings were detected along retracting neurites as soon as 10 minutes after exposure to psychosine, (arrows in Fig. 7h). These swellings were not found in vehicle-treated neurons (Fig. 7i). Psychosine treatment also converged in increased activation of caspase 3, an indicator of apoptosis (Fig. 7j and 7k).

To determine the effects of psychosine on the long-term survival of neuronal cultures, MTT assays were performed on differentiated cultures of cortical neurons exposed to various concentrations of psychosine for 24 hours. Neuronal survival rapidly decreased with psychosine treatment, (Supp. Fig. 4g), which was also accompanied by a sharp loss of neurites (Supp. Fig. 4a-4f). Incubation of neurons with D-sphingosine (used as a control lipid for psychosine) showed no effect on cell survival and/or neurite stability, underlining the specificity of the psychosine pathogenic effect. It seems also important to note, that because we demonstrated that neurons could take psychosine up from exogenous sources (i.e. addition of psychosine to the cell medium), the possibility that in vivo, part of the neuronal psychosine may also originate from non-neuronal sources cannot be completely ruled out.

Specific experiments are currently underway to determine other sources of pathogenic psychosine for neurons.

DISCUSSION

In this work, we present evidence of a dying-back neurodegeneration affecting the nervous system of the Twitcher mouse. Our results also show that psychosine is sufficient to act as a pathogenic molecule to neurons, causing axonal instability and apoptotic cell death.

A dying-back defect in the Twitcher nervous system. In addition to demyelination, axonal and neuronal defects seem to occur in the Twitcher mouse. For example, Twitcher mice show poor development of large diameter axons, [25]. This observation suggests deregulation of cytoskeletal growth [13] and may be caused by an imbalance of neurofilament phosphorylation. Twitcher mice also develop abnormal postural reflexes, grasp and limb strength, and some motor deficiencies, most noticeable in young animals, [35]. We reported damage to neuronal populations in the hippocampus and to axons in the PNS and CNS and in non-neural tissue such as the thymus, [15, 19, 20]. Unfortunately, the pathogenic mechanism causing these neuronal deficits as well as whether or not these are cell autonomous defects have remained undetermined.

To start addressing these questions, we generated a double transgenic Twitcher line (Twi-YFPax), where axons were labeled with YFP. Analysis of these mice revealed swellings, varicosities and even transected fibers in various populations of mutant axons. Similar abnormalities are characteristic pathological profiles of axonal degeneration in other non-related neurological diseases like amyotrophic lateral sclerosis, multiple sclerosis, traumatic brain injury and Parkinson's disease [7, 9, 21, 44]. The identification of axonal dystrophism in the Twitcher mouse indicates the presence of focal points of injury along mutant axons. Interestingly, axonal abnormalities were detected at very early stages of postnatal development (P7), before the onset of demyelination. These pathological findings rapidly progressed in frequency and distribution during ageing. However, neuronal death was

detected only after disease onset, when demyelination was active (e.g. after 30 days of age). This suggests that neuronal death is a late event in the pathophysiology of this disease, likely triggered by a combination of axonal defects, myelin loss, astrogliosis and inflammation. In contrast, axonal dystrophy seems to start much earlier, maybe even at late stages of embryonic development (not examined in this study). This initial evidence is suggesting that a dying-back mode of neuronal pathology may be activated in the nervous system of Krabbe disease. The model of dying back axonopathy proposes that axonal dysfunction precedes the death of the neuronal body. This process seems to start at the synaptic end of the axons, where structural and functional defects begin to impact on synaptic efficiency and then slowly receding towards the body of the neuron [10]. In this respect, one given neuronal body may be anatomically intact while its axon is already dysfunctional. In this model, axonal destruction (loss) may even not be detected. Reports of axonal dystrophy in other leukodystrophies are scarce [34, 38, 45]. In the case of Krabbe disease, reports have been insufficient to bring light into this issue. Several studies have shown that the loss of synapses and axonal injury occur long before neuronal apoptosis and even if apoptosis is prevented [36, 51]. In this respect, our study provides a structural basis to explain some of the neurological disabilities observed in this Krabbe disease mouse model and may be relevant to understand the limitation of current therapies in affected humans.

Psychosine is a pathogenic sphingolipid for neurons. If the progression of Krabbe disease is compounded with a dying back pathology, what is the mechanism of this process? Because psychosine is a lipid raft-associated neurotoxin that accumulates in Krabbe disease [50, 49], it is reasonable to speculate that this neurotoxin will also affect mutant neurons. Our studies examined this possibility in more detail. Psychosine was detected in significant quantities in cultured mutant neurons in the absence of myelinating glia. Neuronal levels of psychosine were significantly lower than those found in cultured Twitcher oligodendrocytes.

The significance of different levels of psychosine in neurons and glia is unclear but it may indicate intrinsic cell-specific mechanisms that regulate how much psychosine is produced in a particular cell type. Differential production of psychosine may also be related to the differential effects of psychosine on different cell populations. For example, psychosine inhibits the last steps of the mitotic cycle in replicating microglia and COS cells, inducing the formation of multinucleated globoid cells [28]. On the other hand, psychosine induces apoptotic cell death in oligodendrocytes [26, 40, 42, 53] and axonal and neuronal degeneration (our study) but not multinuclear phenotypes.

While it is clear that psychosine is toxic for neurons, the origin of the neuronal psychosine is still unclear. Psychosine may reach the axon and neurons from various sources such as i) neuronal synthesis and transport via membrane-bound cargoes; ii) in situ synthesis in the axonal compartment; iii) lipid transfer from myelin and glial cells and iv) extracellular mobilization through circulating vesicles. The synthesis of lipids such as sphingomyelin and phosphatodylcholine has been demonstrated in axons [31] and several works have shown the transport of various lipids and cholesterol along the axon prior to their insertion in the axolemma [47, 46]. Lipid transfer between axons and myelin has also been shown for certain species of lipids [47]. Our results show that mutant granule neurons also contain measurable and significantly high levels of psychosine, indicating endogenous neuronal synthesis, at least in this neuronal type. Whether one or more of these sources contribute to the accumulation of psychosine in axons and neurons is presently unclear but current studies in our laboratory are being conducted to address this question.

Axonopathy contributes to the pathogenesis of Krabbe disease. Knud Krabbe described the first cases of this demyelinating disease in 1916 [30]. In his report, a clear description of diffuse white matter damage was presented. Interestingly, a few indications of neuronal

damage were also reported in his communication as well as in scattered reports that followed, [20, 25, 32, 37, 39], but their significance remained largely uncharacterized. Our study has taken one step into understanding the neuronal component of this disease. Our results, focusing primarily in the spinal cord and sciatic nerves of the Twitcher mouse, indicate the presence of early axonal stress in the absence of demyelination. With the onset of clinical symptoms, these axonal defects increase in frequency and eventually, lead to apoptotic stress of motorneurons in the mutant spinal cord. Our findings show at least two degenerative pathways acting contemporaneously to generate a compounding neuropathology after the onset of the disease (Fig. 8a). In this model, accumulation of psychosine is very high after disease onset, causing toxic degeneration of myelinating glia, demyelination, neuroinflammation and astrogliosis. In this late stage, neuronal stress and death also occur, targeting at least some neuronal populations and producing a compounding neuropathology. However, before disease onset, accumulation of psychosine is low and below the threshold needed to kill glial cells but sufficient to affect the structure of axons, causing a dying-back neuronal defect. Consequently, during the first weeks of life of the mutant, neuronal circuitries may be partially dysfunctional contributing to the mild neurological disabilities described by Olmstead [35]. Axonal swellings maybe caused by inefficient fast axonal transport of membranous bound organelles and by the focal accumulation of unsorted cargoes (Fig. 8b and 8c; Cantuti & Bongarzone, unpublished results). This could lead to an imbalanced distribution of ion channels in mutant axons [14, 23, 27], causing abnormal intra-axonal levels of ions like calcium and sodium and abnormal activation of calcium-dependent calpains and other caspases [4, 54]. Unsafe caspase/calpain levels could trigger degradation of the axonal cytoskeleton, leading to the instability and eventually, transection of axons. This model of neurodegeneration does not require of major losses of axons; axonal projections may be

dysfunctional but still structurally present. In this respect, axonal density in mutant and wild type nerves was found not to be significantly different, [25].

In conclusion, we provide evidence that the Twitcher mouse is affected by an early, progressive axonopathy, operating in a dying-back pattern. While the loss of neurons is a normal event during the embryonic development of the nervous system, its occurrence in early infancy and adulthood is not, bringing irreversible consequences. Our observations of early postnatal neurodegeneration in the Twitcher nervous system may help to understand the limitations of current corrective therapies for this disease.

Figure Legends

Figure 1: Axonopathy in the Twitcher spinal cord. *a-d)* Coronal (a, c) and longitudinal (b, d) sections from postnatal day 30 (P30) wild type (WT)-YFPax and Twitcher (TWI)-YFPax were observed with a confocal microscope to detect axonal dystrophy. VWM: ventral white matter. VH: ventral horn. Insert boxes are higher magnifications from boxed areas in the ventral white matter. Magnification 200x. Red fluorescence is propidium iodine. *e, f)* Longitudinal sections from P30 TWI-YFPax and WT-YFPax were confocally imaged to identify axonal abnormalities. White axons point to swellings and blue arrows to breaks or transected areas in mutant axons. Red fluorescence is propidium iodine. Magnification 650x.

Figure 2: Progressive axonal degeneration in Twitcher axons. Confocal imaging revealed different stages of axonal degeneration in Twitcher axons. Z-stacking confocal imaging was performed on longitudinal sections of P30 spinal cord. White arrows point to three different stages of axonal degeneration in the Twitcher mouse (a-c). Orthogonal reconstructions show the YZ and XZ axes. White lines point to selected axonal alterations. These pathological profiles were not detected in any wild type tissue analyzed. 1000x.

Figure 3: Early signs of axonal dystrophy in the Twitcher mouse. Confocal imaging of longitudinal sections from P7 (a, b) and P15 (c-f) lumbar spinal cords revealed axonal swellings (arrows) at 7 days of age in the Twitcher spinal cord. These pathological profiles were not detected in any wild type tissue analyzed. Magnification 650x.

Figure 4: Axonal degeneration in the Twitcher sciatic nerve. Confocal imaging of longitudinal sections from P7 (a), P15 (b) and P30 (c) sciatic nerves revealed axonal dystrophy in P15 and P30 (arrows) but not in P7 nerves of the mutant mouse. These pathological profiles were not detected in any wild type tissue analyzed. Magnification 650x.

**Figure 5: Neuronal apoptosis in the Twitcher spinal cord. *a, b)* TUNEL staining (green) of wild type (WT) and Twitcher (TWI) P7 (a) and P30 (b) spinal cords revealed the presence of significant cell death in the mutant gray matter only at late stages of the disease (P30) but not in presymptomatic (P7) mice. Magnification 100x. *c-e)* Staining with anti-NeuN (red) antibodies confirmed the neuronal nature of the TUNEL stained (green) cells (arrows) in the grey matter. DAPI (blue) was used to label nuclei. Magnification 400x. *f-k)* TUNEL staining identified glia in the ventral white matter (f-h). TUNEL+ cells were not detected in WT issue (i-k)*. l)* Stereological counting of NeuN+ motorneurons in the ventral horns of the lumbar spinal cord (NeuN+ cells per square millimeter) showed no significant changes in the total number of mutant motorneurons NeuN+ at any time point in postnatal development. N=2-3 animals per group. *m)* Stereological counting of NeuN+ TUNEL+ motorneurons in the ventral horns of the lumbar spinal cord (NeuN+ TUNEL+ cells per square millimeter) showed a significant increase of dying NeuN+ motorneurons in the P30 mutant spinal cord. N=2-3 animals per group.

**Figure 6: Psychosine in Twitcher neurons. *a, b)* Confocal imaging of the CGT enzyme in motor neurons from the ventral horns of the spinal cord of P7 wild type mice. Non-specific binding of secondary antibodies is shown in b. *c)* Western blot analysis of CGT expression levels in lysates from P7 wild type (WT) and Twitcher (TWI) spinal (sp) cords and from NSC34 cells. Actin was used as a loading control. *d)* Real time PCR analysis of GALC and CGT mRNA expression levels in wild type primary cultures of cortical neurons cultured for 3 and 8 day-in vitro (DIV). Results are shown as fold increase respect levels in one DIV cultures. *e-f)* Quantification of psychosine levels in wild type (WT) and Twitcher (TWI) primary neurons by LC-MS-MS. Chromatograms in e show the corresponding peak of psychosine in the Twitcher cells (arrow). WT cells showed traces of the lipid. Quantification of psychosine levels in

neurons and enriched cultures of wild type (white bars) and Twitcher (black bars) oligodendroglia is shown in f.

Figure 7 Psychosine is neurotoxic: *a-d)* Enriched cultures of Twitcher (TWI) and wild type (WT) granule neurons were incubated with cytosine arabinoside for up to 8 days in vitro (DIV) and in the absence of glial cells. Mutant neurons showed signs of degeneration and death by the end of the experiment. *e,f)* LC-MS-MS analysis of psychosine in lipid extracts from NSC34 cells incubated with 10 μM psychosine for 2 hours. *g-k)* NSC34 cells were differentiated for 4 days before exposure to 10 μM psychosine or vehicle for up to 2 hours. Psychosine treatment drastically reduced the number of NSC34 cells with neurites longer than two cell diameters (N=3) (g). The retraction was accompanied by the rapid formation of swellings (arrows in h). This process eventually led to cell death, as shown by the staining for the active fragment of caspase 3 (j, k, in green; red: propidium iodine) in cells treated with psychosine for 60 (j) or 120 (k) min.

Figure 8: Model of compounded neuropathology in the Twitcher mouse. *a)* The progressive accumulation of psychosine is proposed as the main -albeit not necessarily the only- pathogenic trigger in Krabbe disease. Axons become progressively dysfunctional in response to increasing levels of psychosine, generating a dying back neuropathy, which at early postnatal age, is not lethal. Myelinating glia becomes dysfunctional with increasing psychosine and leads to demyelination. After disease onset, neurodegeneration includes neuronal dysfunction and death, creating a compounded neuropathology with very aggressive neurological symptoms. *b-c)* Our study identified various levels of axonal damage in the Twitcher nervous system. These appeared to initiate with axonal varicosities and swellings, which eventually, converge in axonal transections. While the mechanisms that mediate these axonal abnormalities are unclear, we propose that psychosine affects mechanisms regulating

axonal transport and lead to unsafe levels of activated proteases (i.e. calpains, caspases) and imbalance of ions (i.e. calcium and sodium). A combination of one or more of these mechanisms may trigger structural damage and instability of mutant axons.

REFERENCES

1. Aicardi, J. (1993) The inherited leukodystrophies: a clinical overview. J Inherit Metab Dis, 16:733-43.
2. Baker, R.H., J.C. Trautmann, B.R. Younge, K.D. Nelson, and D. Zimmerman (1990) Late juvenile-onset Krabbe's disease. Ophthalmology, 97:1176-80.
3. Banker, G. and K. Goslin (1998) Culturing nerve cells. The MIT Press, Cambridge, Massacusetts, USA.
4. Benn, S.C. and C.J. Woolf (2004) Adult neuron survival strategies--slamming on the brakes. Nat Rev Neurosci, 5:686-700.
5. Boespflug-Tanguy, O., P. Labauge, A. Fogli, and C. Vaurs-Barriere (2008) Genes involved in leukodystrophies: a glance at glial functions. Curr Neurol Neurosci Rep, 8:217-29.
6. Bongarzone, E.R., L.M. Foster, S. Byravan, et al. (1996) Conditionally Immortalized Neural Cell Lines: Potential Models for the Study of Neural Cell Function. Methods, 10:489-500.
7. Cheng, C.L.P., J. T. (1988) The effect of traumatic brain injury on the visual system: a morphologic characterization of reactive axonal change. J. Neurotrauma, 5:47-70.
8. Cleland, W.W. and E.P. Kennedy (1960) The enzymatic synthesis of psychosine. J Biol Chem, 235:45-51.
9. Coleman, M. (2005) Axon degeneration mechanisms: commonality amid diversity. Nat Rev Neurosci, 6:889-98.
10. Coleman, M.P. and V.H. Perry (2002) Axon pathology in neurological disease: a neglected therapeutic target. Trends Neurosci, 25:532-7.
11. Costello, D.J., A.F. Eichler, and F.S. Eichler (2009) Leukodystrophies: classification, diagnosis, and treatment. Neurologist, 15:319-28.
12. Cragg, B.G. (1970) What is the signal for chromatolysis? Brain Res, 23:1-21.
13. de Waegh, S.M., V.M. Lee, and S.T. Brady (1992) Local modulation of neurofilament phosphorylation, axonal caliber, and slow axonal transport by myelinating Schwann cells. Cell, 68:451-63.
14. Decker, H., K.Y. Lo, S.M. Unger, S.T. Ferreira, and M.A. Silverman Amyloid-beta peptide oligomers disrupt axonal transport through an NMDA receptor-dependent mechanism that is mediated by glycogen synthase kinase 3beta in primary cultured hippocampal neurons. J Neurosci, 30:9166-71.
15. Dolcetta, D., S. Amadio, U. Guerrini, et al. (2005) Myelin deterioration in Twitcher mice: motor evoked potentials and magnetic resonance imaging as in vivo monitoring tools. J Neurosci Res, 81:597-604.
16. Dolcetta, D., L. Perani, M.I. Givogri, et al. (2006) Design and optimization of lentiviral vectors for transfer of GALC expression in Twitcher brain. J Gene Med, 8:962-71.
17. Dunn, H.G., B.D. Lake, C.L. Dolman, and J. Wilson (1969) THE NEUROPATHY OF KRABBE'S INFANTILE CEREBRAL SCLEROSIS: GLOBOID CELL LEUCODYSTROPHY. Brain, 92:329-344.
18. Feng, G., R.H. Mellor, M. Bernstein, et al. (2000) Imaging neuronal subsets in transgenic mice expressing multiple spectral variants of GFP. Neuron, 28:41-51.
19. Galbiati, F., V. Basso, L. Cantuti, et al. (2007) Autonomic denervation of lymphoid organs leads to epigenetic immune atrophy in a mouse model of Krabbe disease. J Neurosci, 27:13730-8.
20. Galbiati, F., M.I. Givogri, L. Cantuti, et al. (2009) Combined hematopoietic and lentiviral gene-transfer therapies in newborn Twitcher mice reveal contemporaneous neurodegeneration and demyelination in Krabbe disease. J Neurosci Res, 87:1748-59.

21. Galvin, J.E., Uryu, K., Lee, V. M. & Trojanowski, J. Q. (1999) Axon pathology in Parkinson's disease and Lewy body dementia hippocampus contains α-, β-, and γ-synuclein. Proc. Natl Acad. Sci. USA, 96:13450–13455.

22. Gavrieli, Y., Y. Sherman, and S.A. Ben-Sasson (1992) Identification of programmed cell death in situ via specific labeling of nuclear DNA fragmentation. J Cell Biol, 119:493-501.

23. Gu, Y. and C. Gu Dynamics of Kv1 channel transport in axons. PLoS One, 5:e11931.

24. Igisu, H. and K. Suzuki (1984) Progressive accumulation of toxic metabolite in a genetic leukodystrophy. Science, 224:753-5.

25. Jacobs, J.M., F. Scaravilli, and F.T. De Aranda (1982) The pathogenesis of globoid cell leucodystrophy in peripheral nerve of the mouse mutant twitcher. J Neurol Sci, 55:285-304.

26. Jatana, M., S. Giri, and A.K. Singh (2002) Apoptotic positive cells in Krabbe brain and induction of apoptosis in rat C6 glial cells by psychosine. Neurosci Lett, 330:183-7.

27. Kagitani-Shimono, K., I. Mohri, T. Yagi, M. Taniike, and K. Suzuki (2008) Peripheral neuropathy in the twitcher mouse: accumulation of extracellular matrix in the endoneurium and aberrant expression of ion channels. Acta Neuropathol, 115:577-87.

28. Kanazawa, T., S. Nakamura, M. Momoi, et al. (2000) Inhibition of cytokinesis by a lipid metabolite, psychosine. J Cell Biol, 149:943-50.

29. Karnes, H.E., C.L. Kaiser, and D. Durham (2009) Deafferentation-induced caspase-3 activation and DNA fragmentation in chick cochlear nucleus neurons. Neuroscience, 159:804-18.

30. Krabbe, K. (1916) A new familial, infantile form of diffuse brain. sclerosis. Brain, 39:74-114.

31. Krijnse-Locker, J., R.G. Parton, S.D. Fuller, G. Griffiths, and C.G. Dotti (1995) The organization of the endoplasmic reticulum and the intermediate compartment in cultured rat hippocampal neurons. Mol Biol Cell, 6:1315-32.

32. Kurtz, H.J. and T.F. Fletcher (1970) The peripheral neuropathy of canine globoid-cell leukodystrophy (krabbe-type). Acta Neuropathol, 16:226-32.

33. Nagara, H., T. Kobayashi, K. Suzuki, and K. Suzuki (1982) The twitcher mouse: normal pattern of early myelination in the spinal cord. Brain Res, 244:289-94.

34. Ohara, S., Y. Ukita, H. Ninomiya, and K. Ohno (2004) Axonal dystrophy of dorsal root ganglion sensory neurons in a mouse model of Niemann-Pick disease type C. Exp Neurol, 187:289-98.

35. Olmstead, C.E. (1987) Neurological and neurobehavioral development of the mutant 'twitcher' mouse. Behav Brain Res, 25:143-53.

36. Sagot, Y., M. Dubois-Dauphin, S.A. Tan, et al. (1995) Bcl-2 overexpression prevents motoneuron cell body loss but not axonal degeneration in a mouse model of a neurodegenerative disease. J Neurosci, 15:7727-33.

37. Schlaepfer, W.W. and A.L. Prensky (1972) Quantitative and qualitative study of sural nerve biopsies in Krabbe's disease. Acta Neuropathol, 20:55-66.

38. Schnorf, H., R. Gitzelmann, N.U. Bosshard, M. Spycher, and W. Waespe (1995) Early and severe sensory loss in three adult siblings with hexosaminidase A and B deficiency (Sandhoff disease). J Neurol Neurosurg Psychiatry, 59:520-3.

39. Sourander, P. and Y. Olsson (1968) Peripheral neuropathy in globoid cel leucodystrophy (morbus Krabbe). Acta Neuropathol, 11:69-81.

40. Suzuki, K. (1998) Twenty five years of the "psychosine hypothesis": a personal perspective of its history and present status. Neurochem Res, 23:251-9.

41. Suzuki, K. and K. Suzuki (1990) Myelin pathology in the twitcher mouse. Ann N Y Acad Sci, 605:313-24.
42. Tanaka, K. and H.D. Webster (1993) Effects of psychosine (galactosylsphingosine) on the survival and the fine structure of cultured Schwann cells. J Neuropathol Exp Neurol, 52:490-8.
43. Taniike, M., I. Mohri, N. Eguchi, et al. (1999) An apoptotic depletion of oligodendrocytes in the twitcher, a murine model of globoid cell leukodystrophy. J Neuropathol Exp Neurol, 58:644-53.
44. Tsai, J., J. Grutzendler, K. Duff, and W.B. Gan (2004) Fibrillar amyloid deposition leads to local synaptic abnormalities and breakage of neuronal branches. Nat Neurosci, 7:1181-3.
45. van der Voorn, J.P., W. Kamphorst, M.S. van der Knaap, and J.M. Powers (2004) The leukoencephalopathy of infantile GM1 gangliosidosis: oligodendrocytic loss and axonal dysfunction. Acta Neuropathol (Berl), 107:539-45.
46. Vance, J.E., R.B. Campenot, and D.E. Vance (2000) The synthesis and transport of lipids for axonal growth and nerve regeneration. Biochim Biophys Acta, 1486:84-96.
47. Vance, J.E., D. Pan, R.B. Campenot, M. Bussiere, and D.E. Vance (1994) Evidence that the major membrane lipids, except cholesterol, are made in axons of cultured rat sympathetic neurons. J Neurochem, 62:329-37.
48. Wenger, D.A., M.A. Rafi, P. Luzi, J. Datto, and E. Costantino-Ceccarini (2000) Krabbe disease: genetic aspects and progress toward therapy. Mol Genet Metab, 70:1-9.
49. White, A.B., F. Galbiati, M.I. Givogri, et al. (2011) Persistence of psychosine in brain lipid rafts is a limiting factor in the therapeutic recovery of a mouse model for Krabbe disease. J Neurosci Res, 89:352-64.
50. White, A.B., M.I. Givogri, A. Lopez-Rosas, et al. (2009) Psychosine accumulates in membrane microdomains in the brain of krabbe patients, disrupting the raft architecture. J Neurosci, 29:6068-77.
51. Whitmore, A.V., T. Lindsten, M.C. Raff, and C.B. Thompson (2003) The proapoptotic proteins Bax and Bak are not involved in Wallerian degeneration. Cell Death Differ, 10:260-1.
52. Wijsman, J.H., R.R. Jonker, R. Keijzer, C.J. van de Velde, C.J. Cornelisse, and J.H. van Dierendonck (1993) A new method to detect apoptosis in paraffin sections: in situ end-labeling of fragmented DNA. J Histochem Cytochem, 41:7-12.
53. Zaka, M. and D.A. Wenger (2004) Psychosine-induced apoptosis in a mouse oligodendrocyte progenitor cell line is mediated by caspase activation. Neurosci Lett, 358:205-9.
54. Zalewska, T., M. Kanje, and A. Edstrom (1986) A calcium-activated neutral protease in the frog nervous system which degrades rapidly transported axonal proteins. Brain Res, 381:58-62.

Cantuti et al., 2011 Fig. 1

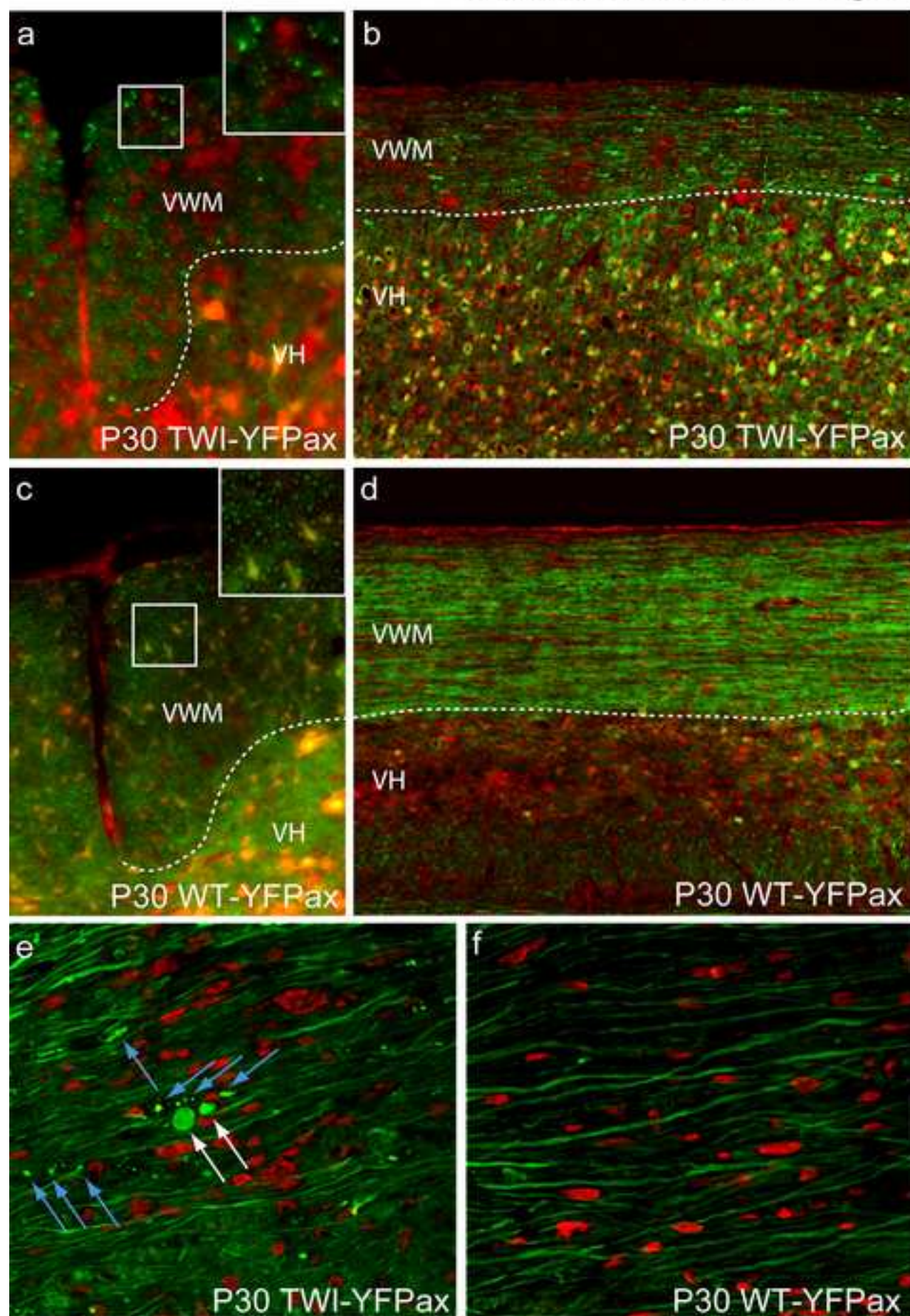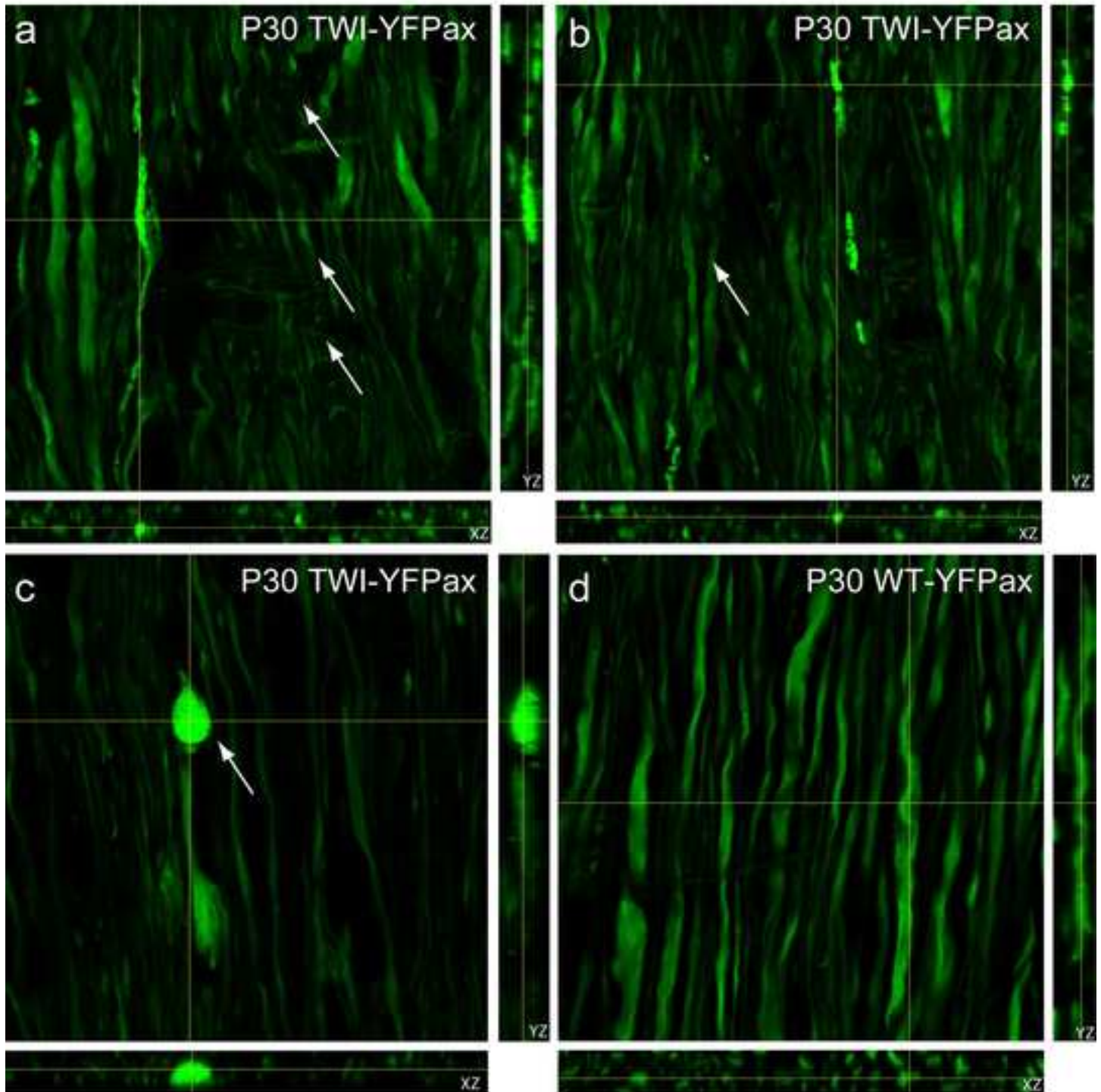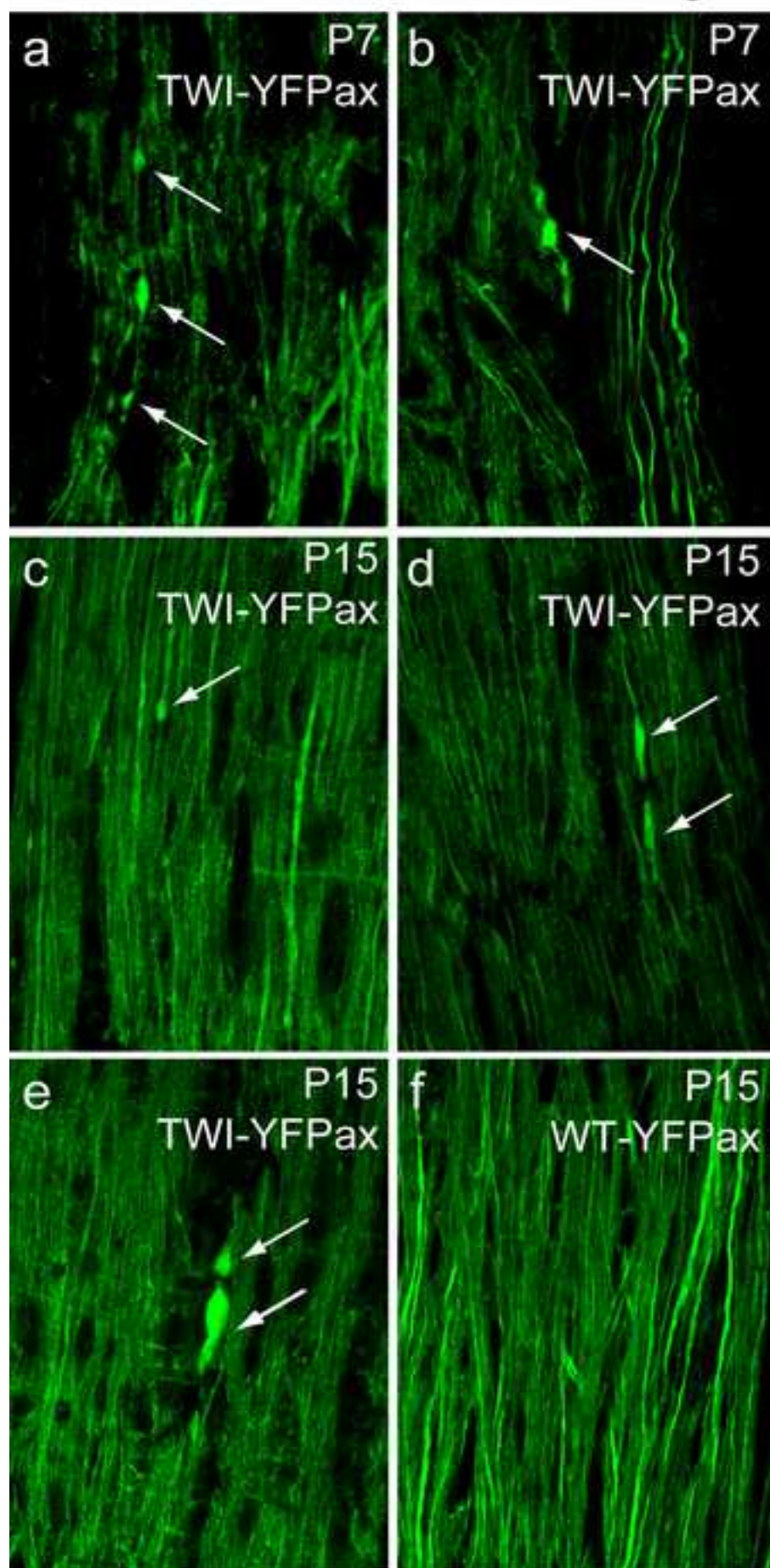Cantuti et al., 2011 Fig. 2

Cantuti et al., 2011 Fig. 3

figure 4
Click here to download high resolution image

Cantuti et al., 2011 Fig. 4
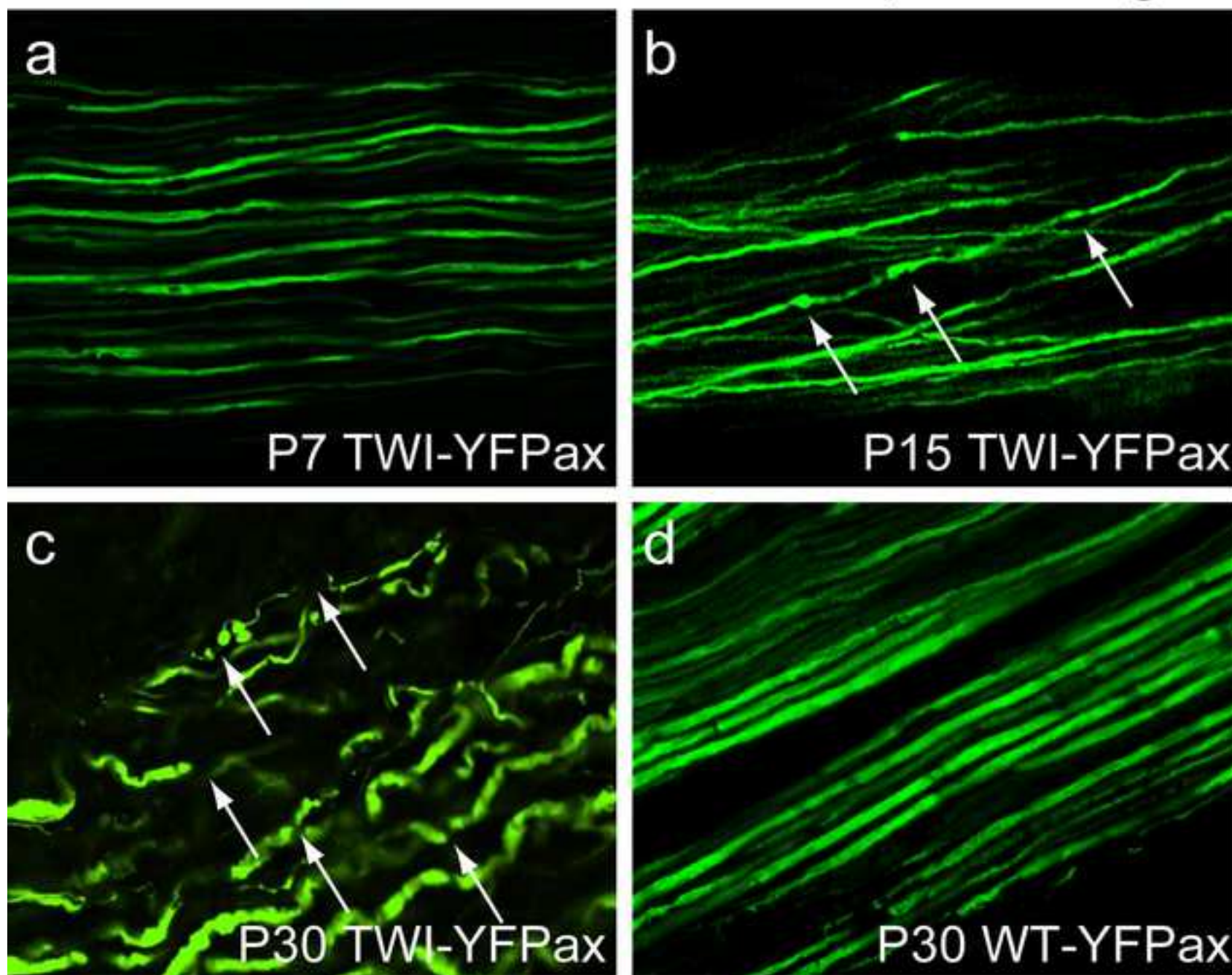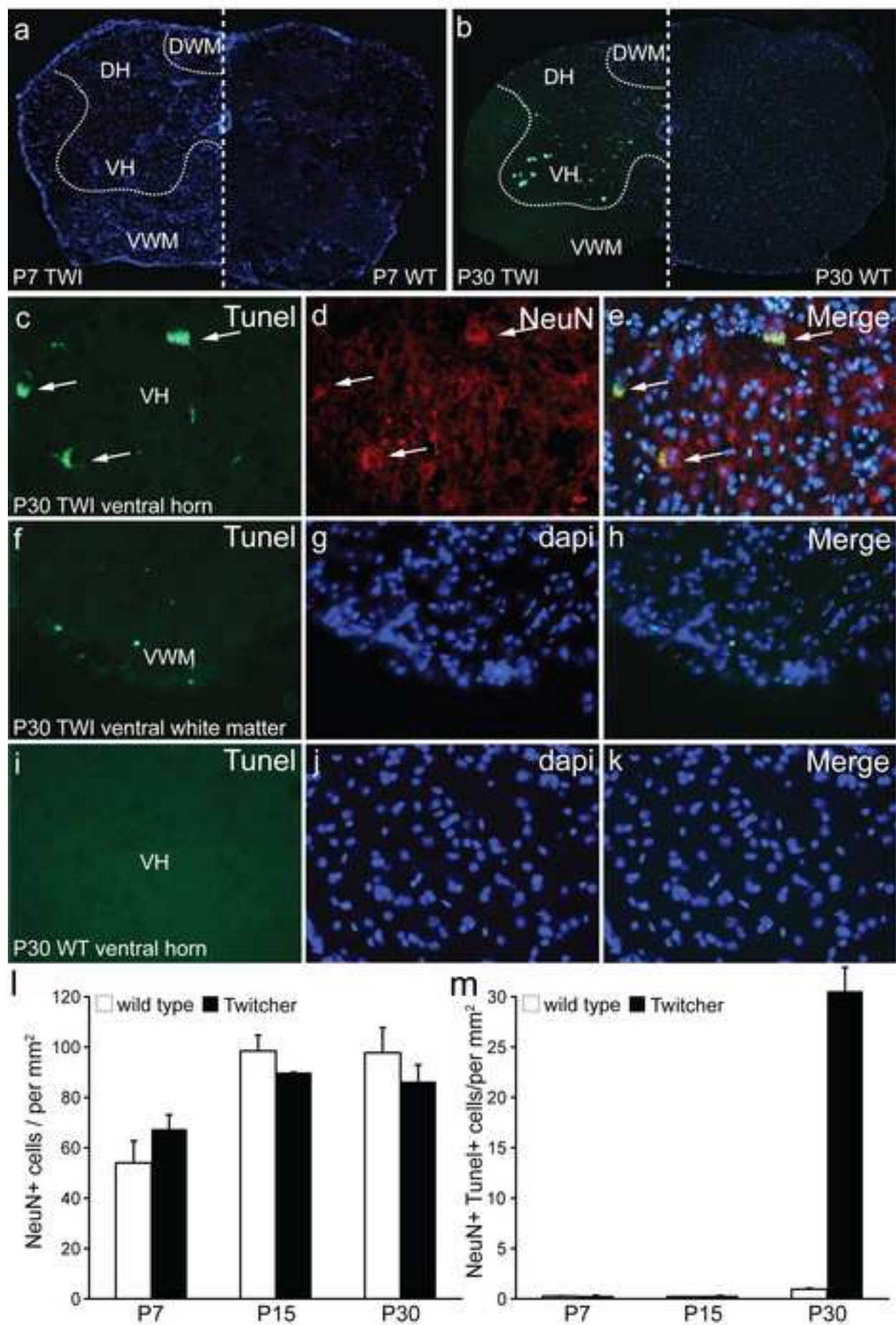
Cantuti et al., 2011 Fig. 5
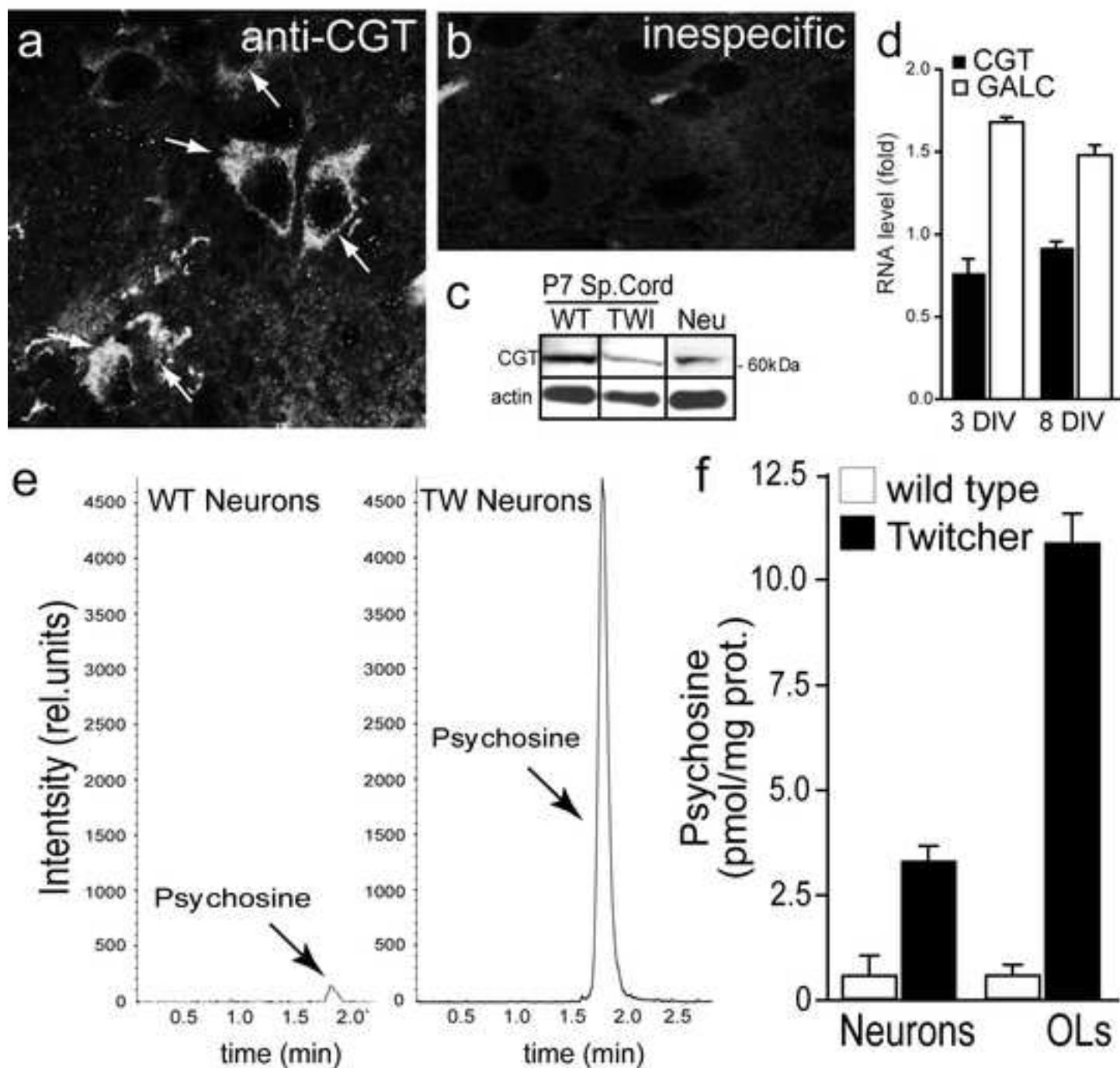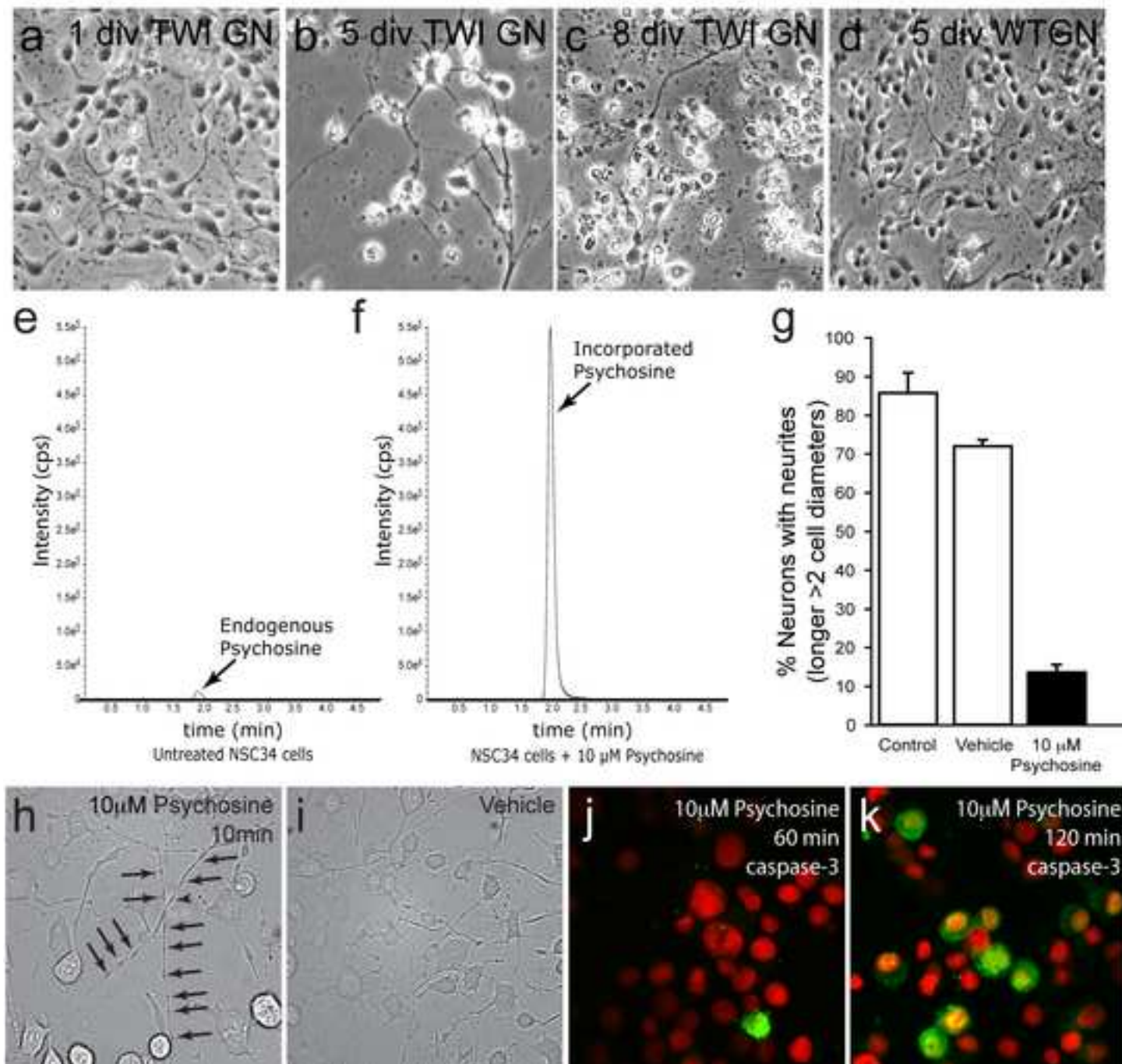
Cantuti et al., 2011 Fig. 6

Cantuti et al., 2011 Fig. 7

Cantuti et al., 2011 Fig. 8